The structural assessment of sandwich panels with 3D printed cores for spacecraft applications

Adrian Dumitrescu(1), Scott J. I. Walker(2), Federico Romei(3), Atul Bhaskar(4)

(1) *University of Southampton; University Road, Southampton, SO17 1BJ, UK; ad2g15@soton.ac.uk*
(2) *University of Southampton; University Road, Southampton, SO17 1BJ, UK; sjiw@soton.ac.uk*
(3) *University of Southampton; University Road, Southampton, SO17 1BJ, UK; f.romei@soton.ac.uk*
(4) *University of Southampton; University Road, Southampton, SO17 1BJ, UK; a.bhaskar@soton.ac.uk*

KEYWORDS: Additive Manufacturing, 3D Printing, Sandwich Panels, Satellite Structures, ReDSHIFT

ABSTRACT

This study aims to investigate the use of Additive Manufacturing (AM) for spacecraft structural design and it focuses on a 3D printed approach to the standard sandwich panel honeycomb core. The CFRP facesheets are already highly optimized constructions that can hardly be improved by 3D printing. In contrast, the core has a lot of potential for improvement. Standard Aluminium honeycomb cores, while being structurally efficient, have fixed geometries that cannot be varied throughout the panel. It is also very labour intensive and structurally problematic to incorporate the necessary inserts into a structural panel and printing can help improve both structural and manufacturing aspects.

The objective of this paper is to compare sandwich panels with CFRP facesheets and 3D printed Aluminium core to a standard sandwich panel construction and characterize the performance variation from the baseline. The effect of varying core to facesheet contact area on stiffness is also assessed. These comparisons are from 18 of the 208 total samples which were manufactured as part of the EU funded ReDSHIFT project. The samples were subjected to three point bending (3PB) and compression tests. Strength and stiffness as well as the failure modes of all the samples are investigated. Experimental results are compared to both theoretical predictions and simulations produced in ANSYS 2019 R2. The porosity of the 3D printed cores is also discussed because issues concerning the density of the end product appear for low wall thickness cores.

1 INTRODUCTION

The honeycomb core sandwich panel is one of the most widely used structural configurations in satellite structures today. The combination of very stiff facesheets with a lightweight core that helps take the stiff faces away from the neutral axis leads to a highly efficient structure in both bending and compression. The sandwich concept affords a significant increase in flexural rigidity and bending strength with a low mass penalty. Mass saving and high specific properties are key considerations in spacecraft design since it costs around $10,000 per pound to put a payload in orbit[1].

1.1 Standard Panel Issues

In most cases, space grade honeycomb core sandwich structures are made up of CFRP facesheets and an Aluminium core. The cost, time and complexity of manufacturing such an assembly are high, especially when adding features such as inserts. Most of the complexity comes from manufacturing of the core, for which there are several methods. One of the most popular involves bending of Aluminium sheets as desired, followed by bonding of strips. The bonded product is pulled apart to create the expanded panel. This method introduces anisotropy in the structure, as honeycomb cell walls parallel to the ribbon direction are double in thickness compared with the rest. Moreover, for high relative density cores, the force needed to stretch the metal eventually approaches the inter-sheet bond fracture strength. This leads to a second manufacturing method that takes the Aluminium sheet and it runs it through a gear press to obtain the desired corrugations. Corrugated sheets are then welded together and the large corrugated blocks are cut into corrugated cores. The double wall anisotropy remains[2].

Apart from being complex and involving several tools and welding procedures, these traditional manufacturing processes restrict freedom in design. The parameters that the designer can set are the cell geometry, cell size (which involves relative density) and the core height. Properties are fixed across the honeycomb which leads to a sub-optimal structure. A solution while using honeycomb cores is the use of AM.

Metal 3D printing, and Aluminium printing in particular, can revolutionize honeycomb core design in two

ways. Firstly, it can lower time, cost and manufacturing complexity by replacing a multi-step process with one that only involves one printer and the technicians to set it up. Secondly, it offers design freedom which can lead to more optimized honeycomb structures, better specific strength and stiffness and an overall lower mass. As a result, it is essential to start to understand the relative structural performance of a printed core compared to the standard baseline honeycombs used today.

1.2 The ReDSHIFT Investigation

Part of the project focus was on the impact that AM can have on mass, volume, time and cost saving in the context of the next generation of satellites. Using a standard 1000 kg LEO satellite as the baseline, it was determined that the subsystems that can benefit from AM are: baseplate, structure, equipment and harness. The four make up 59% of the total system mass, so only a 20% decrease in mass due to AM leads to an 11.8% overall mass reduction, or potentially 100 kg+ more for payload[3].

ReDSHIFT[3] was perhaps the first project to investigate 3D printed Aluminium honeycomb cores attached to CFRP facesheets. Test panels were manufactured using AlSi10Mg SLM printed cores and TORAY M55J pan graphite/EX-1515 laminate CFRP. The panels were subjected to three-point-bending (3PB) and compression and the contact area between the adhesive and the core was varied to assess its impact on sample stiffness. To act as a baseline, a standard Al 5056 Hexcel honeycomb core sandwich panel was subjected to the same loading scenarios. Strength, stiffness and failure modes of all samples are investigated here.

2 EXPERIMENTAL RESULTS

The sample types investigated in 3PB and compression are presented in Table 1. A key parameter for the 3D printed cores is the wall thickness. The manufacturers' recommended minimum print thickness was 1 mm. Initial trial prints were performed to determine the minimum print thickness that could reliably be achieved without significant print flaws occurring. This resulted in the selection of the 300 μm wall thickness. Although this results in a mass increase with respect to the standard baseline core, it represents the lightest comparative 3D printed solution using the same basic honeycomb geometry for comparative purposes. Also, note that the CFRP facesheet thickness was 0.64 mm in all cases and that the free span of the 3PB tests is 150 mm.

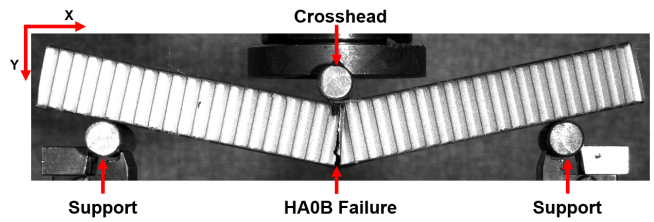

Figure 1: 3PB Experimental Setup - HA0B at Failure

For all experiments, the failure load was reported from the INSTRON load cells in the test machines (INSTRON 5560 for 3PB and INSTRON 4204 for compression) with sampling every 0.1 seconds. Displacement is captured using image tracking in ImageJ with a frame every 0.2 - 1 second. The displacement reported by INSTRON can be inaccurate because it includes the displacement of the machine itself, while point tracking isolates the sample displacement. Due to the lower sampling rate, the imaging data may miss the true load peaks, whereas the INSTRON provides this data at a higher sampling rate.

Two types of error bars will be reported. One of them shows the variation in load or displacement for similar samples undergoing the same loading scenario.

Core Type	Core Details	Sample Dimensions	# Samples	Name
Baseline Honeycomb Core	Cell Size: 4.8 mm Wall Thickness: 18 μm Core Density: 32 kg/m^3	3PB: 200 mm × 75 mm × 20.68 mm Comp: 80 mm × 80 mm × 20.68 mm	5 3PB 5 Comp	HSNB 1 - 5 HSNC 1 - 5
Standard Printed Honeycomb Core	Cell Size: 4.8 mm Wall Thickness: 300 μm Core Density: variable	3PB: 200 mm × 75 mm × 20.68 mm Comp: 50 mm × 50 mm × 20.68 mm	2 3PB 3 Comp	HA0B 1 - 2 HA0C 1 - 3
Printed Core with Varying Contact Area	Contact Area: 25%, 50%, 75%	3PB: 200 mm × 75 mm × 20.68 mm	3 3PB	HA1B HA2B HA3B

Table 1: Main properties of the experimental samples

The second shows the displacement variation between several points tracked on the same sample. The latter is used to confirm that point tracking was done at reliable and robust locations such as the cross-head and the supports where virtually no body displacements occur.

2.1 Three Point Bending

The 3PB samples are listed in Table 1 and their denominations are HSNB/HA0B/HA1B/HA2B/HA3B. *H* stands for honeycomb, *SN* and *A* for standard baseline and additively manufactured core respectively, *0 - 3* identifies the type of printed core and *B* stands for bending. They are the same in compression with *C* instead of *B*.

The main point of interest was the sample behaviour before failure, which is the linear part of the force-displacement curve. This should give information related to both the strength and the stiffness of the samples in order to assess the effectiveness of both using printing and varying adhesive contact size on standard printed honeycombs when compared to the baseline. The experimental results reported below are averaged over multiple samples of the same type for HSNB and HA0B. The sample error is given by the difference between the average load or displacement value and the experimental extremes. The image error is the average frame by frame displacement error between the 3 points tracked in ImageJ on the same sample.

Table 2 presents absolute values for both maximum load and displacement at failure. Before specific values are reported and analyzed, this data can be studied qualitatively to compare the force-displacement curves of HSNB and HA0B. This should give an insight into the main differences between a baseline and a printed core, as they are the most basic examples of the two categories.

Figure 2 shows the average values of the experimental force-displacement data for the baseline honeycomb core (HSNB) and the standard printed core (HA0B) in bending. Both curves in Figure 2 have the general outline of the expected force - displacement relation for a 3PB experiment done on sandwich structures. The linear elastic region between the start of the experiment and the peak load where the samples fail can be observed. There is a rapid drop in the applied load followed by a flattening out of the curve and even a slight load increase with the increasing sample displacement. This is because after failure, the honeycomb walls tend to fold out, but they are constrained and quickly reach a local densification point that causes the applied load to stabilize[4]. Having observed that both samples generally behave as expected, their differences can be explored in greater depth.

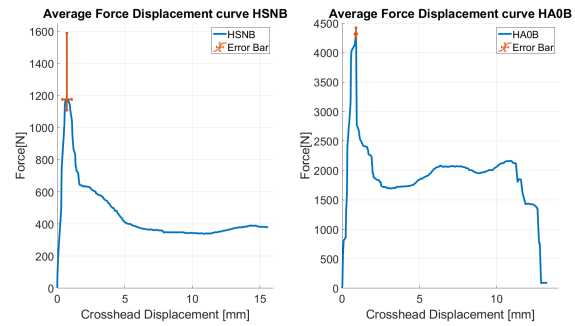

Figure 2: Force Displacement Curve for HSNB and HA0B. Plot based on imaging data only.

Focusing on the linear sections of the two plots, HSNB has a much smoother curve compared to that for HA0B and, therefore, the former shows a relatively more elastic behaviour before failure. The HA0B curve exhibits displacement step jumps during loading. At several loading points, the sample displaces significantly under the cross-head before it continues to resist the load applied. Given the sample porosity of around 50%, it can be inferred that the printed core might fail sequentially as micro-cracks release energy through a rearrangement of the microstructure within the material.

Sample	Failure Load (N)	Sample error (N)	Vertical Y displacement at failure (mm)	Sample error (mm)	Image error (mm)
HSNB	1252.16364	-118.36 +349.55	0.685252	-0.322 +0.404	±0.03256
HA0B	4534.68435	±82.81	0.99857	±0.15506	±0.024189
HA1B	4861.9844	N/A	0.8179	N/A	±0.0107
HA2B	5489.4155	N/A	0.72708	N/A	±0.1904
HA3B	7629.2588	N/A	1.026	N/A	±0.0245

Table 2: Experimental results for 3PB

Sample	Average sample weight (g)	Sample stiffness (N/mm)	Sample specific stiffness (N/(mm × g))
HSNB	41.13	1827.304	44.42752
HA0B	78.72	4541.178	57.6877
HA1B	83.32	5944.473	71.345
HA2B	97.04	7549.947	77.8024
HA3B	116.09	7435.925	64.0531

Table 3: Mass and stiffness of 3PB samples

At certain load levels, the core material rearranges locally after significant vertical displacement and then it continues to take increasing loads until the next event occurs. The exact mechanism behind this sequential failure requires further investigation using 3D scanning.

It can be concluded that there is a clear difference between the failure mechanism of a standard baseline honeycomb core that has a single energy release at failure and the printed core that exhibits local failures which release energy before the entire sample collapses.

The sample behaviour at peak load is also contrasting. The response of HSNB has a plateau around its failure load, which means that the sample undergoes significant displacement under this load before it actually fails. This shows a more robust behaviour close to failure compared to HA0B which fails abruptly after the peak load is reached. It may be inferred that the printed core is significantly less stable around failure and has a more catastrophic yield.

To get a better idea of sample performance, absolute and relative stiffness are assessed. To this end, all samples were weighed and the values in Table 3 indicate that all printed samples are heavier than the standard honeycomb sandwich panel. This is due to the thicker cell walls imposed by printing. However, the samples are not as heavy as predicted due to porosity (see Section 3).

The standard printed sample, HA0B, has a superior specific stiffness compared to the baseline panel, HSNB. This fact alone already shows the potential of printing for honeycomb cores. In terms of varying the adhesive contact area, the steepest improvement is seen between the regular structure and one with 25% contact area, HA1B. There is a performance peak for 50% contact area, or HA2B as denoted. The potential of printing in the context of honeycomb structures is further confirmed as performance gains are obtained by taking advantage of the manufacturing technique through simple geometry changes. Many more design variations are possible through printing and performance gains are expected going forward, with the caveat that more needs to be understood regarding failure behaviour to reduce the safety factors needed for such samples and regarding printing consistency at low wall thicknesses.

2.2 Compression

A summary of the compression tests can be seen in Table 1. Similar to the bending experiments, the focus point of the compression tests was the sample behaviour before failure. It gives insight into the strength and stiffness comparison between baseline and printed honeycomb cores. The experimental results reported are averaged across the multiple samples of the same type and both sample and image errors are reported in Table 4.

While the failure load variation is relatively small (between -6.67% and +13.27%), the vertical displacement variation is significant and this has an impact on evaluating the sample stiffness. When looking at the data straight from the Instron machine, the force - displacement plots look very smooth and they predict significantly higher displacements compared to those reported in Table 4. However, when looking at the image data and after subtracting the evident relative movement of the sample support, one is left with very small displacements at failure.

Sample	Failure Load (N)	Sample error (N)	Y displacement at failure (mm)	Sample error (mm)	Image error (mm)
HSNC	8102.45196	-542.81 +482.68	0.054	-0.0479 +0.0541	±0.01788
HA0C	20612.71613	-1928.39 +2735.98	0.018849	-0.03276 +0.04885	±0.013767

Table 4: Experimental results for compression

A relatively small sample error of about ± 0.05 mm becomes significant because the average absolute displacement value is of the same magnitude.

As a result of the significant motion of the support, one of the HA0C samples has a measured negative displacement at failure, which is nonsensical. All HSNC samples exhibit a net negative vertical displacement for a significant portion of the force - displacement curve. The experimental shortcomings are evident and to fully observe this highly non-linear sample behaviour, the full test data for all specimens is shown in Figures 3 and 4.

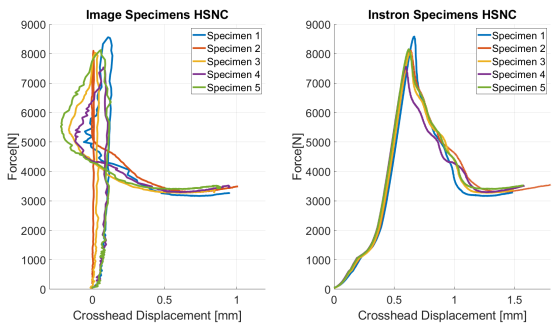

Figure 3: Force Displacement Curve HSNC Image and Instron data

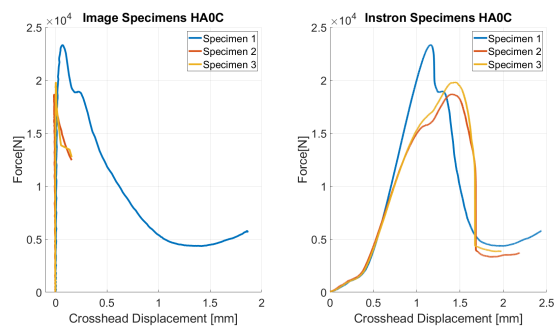

Figure 4: Force Displacement Curve HA0C Image and Instron data

It is clear from the figures above that the imaging data is simply the Instron data with the bottom support movement subtracted, so the plots are pushed to the left. For HSNC, the support movement is so significant that all specimens exhibit a net negative displacement of up to -0.25 mm, as seen in Figure 3. The stiffness of the samples was significant in relation to the experimental setup, so the data reported includes the relative movement of the entire system. However, relative sample stiffness between the baseline and the printed core can still be evaluated qualitatively even if the absolute numbers are not to be trusted entirely.

To begin with, an 80 x 80 mm printed sample could not be crushed in compression by the 50 kN Instron machine as the failure load exceeded the limit of the load cell. The sample size was consequentially reduced to 50 × 50 mm. This fact alone indicates that the printed sample is stronger than the standard honeycomb (even when accounting for HA0C being 1.57 times heavier than HSNC for an 80 x 80 mm sample). This is confirmed by the data in Tables 4 and 5 which gives a specific failure load of 450 N/g for HSNC and 1875 N/g for HA0C. Strength data is very reliable for this set of experiments and partly confirms the potential benefits of having printed cores with thicker walls in compression.

Once again, specific stiffness values are very relevant for direct comparison between the standard baseline core and the 3D printed core. The samples were weighed and the results in Table 5 followed.

Sample	Average weight (g)	Stiffness (N/mm)	Specific stiffness (N/(mm × g))
HSNC	18	150045.4067	8335.856
HA0C	11.09	1093570	98608.72916

Table 5: Mass and stiffness of compression samples

The printed core comes out to be more than 10 times stiffer than its baseline counterpart. Even if there is clear uncertainty in the displacement data, there is a strong indication that a printed core is stiffer than a baseline core. The stiffest HSNC sample (with a significantly outlying reported vertical displacement of 6.1×10^{-3} mm) is still 25% less stiff than the average value obtained for HA0C. Given that generally stiffness scales with the cube of wall thickness, it makes sense for a printed core with a wall 16.6 times thicker than a baseline version to be significantly stiffer. All in all, one can confidently conclude that in compression, a 3D printed core is both stronger and stiffer than a standard baseline counterpart and this further reinforces the future potential of using AM in spacecraft primary structures.

3 POROSITY

Porosity will now be discussed since the experimental samples showed significant porosity levels and because porosity has an important effect on the material properties used later in the theoretical and FEA predictions (Sections 4 and 5).

3.1 Porosity Level and Wall Thickness

In order to assess the dependence of porosity levels on sample wall thickness, two courses of action were taken. First, all the sandwich panels with printed cores from the ReDSHIFT test campaign along with an optimized 3D printed bracket made from the same material (AlSi10Mg) were weighed. The bracket has a minimum wall thickness of 2.7 mm, while in general the thickness is between 3 mm - 6.5 mm, and it can act as a baseline for the rest of the samples. The sample mass gives valuable insight into the porosity level found in all the parts. The second step was to conduct CT scans of a few 3D printed honeycombs as well as of the bracket in order to back up the data obtained through Archimedes' method, while also better understanding the pore distribution and size.

Based on the weight of the samples and on the CFRP and the Hexcel adhesive data sheets, the porosity level varies between 33% and 66% across the printed honeycomb cores. This is a significant porosity level, especially compared to the bracket, which based on its weight has less than 1% porosity (as expected for a part printed with reasonable wall thicknesses). This set of results already exposes some of the issues that come with printing very thin Aluminium structures.

Next, CT scans were performed on two representative parts: an 80 mm x 40 mm sandwich panel with a printed honeycomb off-cut and a 3D printed bracket. The two were scanned in the μvis laboratory, a facility within the School of Engineering at Southampton. The scans were performed on the modified 225 kVp Nikon/Xtek HMX machine at a resolution that scales with the part diameter. The sandwich panels had a resolution of around 50 μm, while the bracket had a resolution of around 80 μm. As was indicated by Archimedes' method, the bracket does not seem to have any noticeable pores. Moreover, the dimensions of the printed part match the CAD dimensions within a tolerance of the image resolution. Hole sizes and wall thicknesses were inspected.

The honeycomb walls are riddled with pores across the two samples and most walls seem to have a long porous section along one of their sides (see Figure 5). This can seriously weaken the contact between the honeycomb walls.

Based on the inspection of a few walls, the areal porosity (pore area divided by total area) came out to be between 10 and 15%. This is far from the 33% - 66% obtained by weighing the samples. One reason for the discrepancy may be that the scanned samples were not part of the weighing investigation because it only focused 3PB and compression specimens which could not give valuable CT scan data due to their previous experimental damage. A more likely cause for the difference is the relatively low resolution of the scans. It is very likely that one could only observe the very large pores since their size can go down to a few μm. Most of the observed pores have sizes between 100 - 300 μm and they generally seem to be circular. Higher resolution is needed to observe the smaller pores and more details of the porosity.

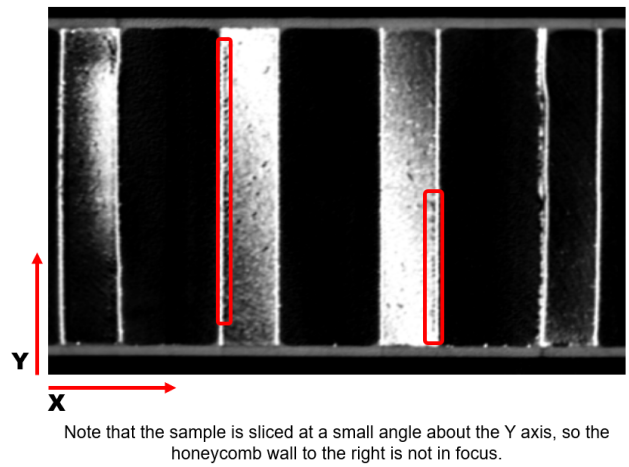

Figure 5: CT scan detail of the 3D printed honeycomb sample. Porous sections along the honeycomb sides are highlighted in red.

This investigation has confirmed that the porosity level in a metal 3D printed part is highly dependent on the wall thicknesses found in the sample. When trying to go down below the 1 mm barrier, porosity will increase significantly and it will play an important role in the mechanical properties of the structure in question. This is why mechanical properties predicted by analyzing purpose-built test samples cannot be relied upon. The data is available for the material and the printers used in ReDSHIFT, but it is not representative of the actual performance of thin-walled AlSi10Mg. Based on the information gathered, such as porosity level and pore size, one could attempt to predict the real mechanical properties of AlSi10Mg in the context of our samples.

3.2 Impact of Porosity on Properties

The main material property that needs to be characterized for any given material is Young's Modulus (E). As mentioned, data is available on the Young's Modulus of AlSi10Mg printed on the printers used in the ReDSHIFT

project (E is about 67 GPa, as expected), but this data is not relevant at low wall thicknesses. What needs to be determined is how Young's Modulus (and shear modulus) scales with porosity and how the real value for our samples can be related to the test samples.

A significant amount of experimental work has been done on finding the effect of porosity on E and in 2013 Choren et al.[5] have summarized the relationship between the two with a focus on AM applications. The equations relating E_P, E_0 and P (E of the porous material, E of the solid material and the porosity level) are of various types: linear, power laws and exponential. Each equation of the 14 they list has been developed with a range of materials and of porosities in mind. All involve constants that are determined experimentally, all generally break down beyond 20% porosity and all can hardly be generalized[6]. As a result, one has to focus on mechanics-based models.

In 1957, J. D. Eshelby[7] looked into the elastic field of an ellipsoidal inclusion and its effect on the stress and strain distribution in and around the inclusion. Based on the work by Eshelby, Luo and Stevens[8] have developed a micromechanical model of randomly oriented ellipsoidal inclusions in composites. They make use of the Eshelby tensor and they relate the elastic moduli of the composites to the matrix moduli for both rigid and soft inclusions. Our case pertains to the soft inclusion category. The relevant equations are

$$\begin{aligned} K_{IM} &= K_M(1-F)/\left(1-F+F\eta_1\right) \\ G_{IM} &= G_M(1-F)/\left(1-F+F\eta_2\right) \end{aligned} \tag{1}$$

where F is the fibre volume fraction and where η_1 and η_2 are related to the shape of the inclusions and depend on components of the Eshelby tensor (more details in[7] [8]).

Based on Eq. (1), Luo and Stevens[8] later determine the effect of ellipsoidal pores on the Young's Modulus of a porous material. They replace the fibre fraction with a pore fraction and use the well known relations between the three elastic moduli and obtain

$$E = \left\{1 + \frac{\left[(1-2\nu)\eta_1 + 2(1+\nu)\eta_2\right]F_p}{3\left(1-F_p\right)}\right\}^{-1} E_0 \tag{2}$$

where F_p is the volume fraction of the ellipsoidal pores. This is an equation based on the micromehanics of inclusions that clearly relates the Young's Modulus of the porous material to the Young's Modulus of the solid material and the pore fraction.

Based on Eshelby's work, Vavakin and Salganik[9] took the analysis further and considered a porous medium with spherical pores of n different radii. It is not expected for all the pores to be the same size, so this addition is relevant. Based on this model, one ends up with a more familiar relation between E and E_0: $E = E_0(1-p)^2$ and $\nu = 0.2$. They show that Poisson's ratio $\nu \to 0.2$ as $p \to 1$, but they choose to keep ν constant at 0.2 for simplicity. This model is the starting point for the work done by Manoylov, Borodich and Evans[10]. Their focus is on modeling the elastic properties of sintered porous materials, which fits in perfectly with our interests. In this paper[10], the authors first check the assumption of uniform distribution of pore sizes of the Vavakin and Salganik (VS) model. They find that for 10 different distributions, the variation in E is less than 1% at porosities below 70%.

The next step was to check the VS model against experimental data for various materials. The VS model applies well to natural porous materials and synthetic foams. This is the case because, based on sample inspection, the pores are roughly spherical and isolated for this kind of materials. However, for sintered materials the model overpredicts E and this can be due to the more varied pore shapes and due to pore merging found in their metallographic cross sections. At this point, Manoylov, Borodich and Evans extend on the VS model and include the merged pores on top of the isolated spherical pores. They do so by calculating the probability that in a given volume, a pore of a certain radius can merge with pores of any other radius in the given radius range. The merged pores are assumed to form an ellipse with the semi-major axis equal to the sum of their radii. This is where the work by Luo and Stevens[8] comes in because the merged pores act as randomly oriented elliptic inclusions and follow Eq. (2).

When compared with experimental data, this model predicts the evolution of E with porosity level for sintered materials much better. As a result, it is deemed appropriate to implement it in the present research to predict the Young's Modulus for each sample tested based on its porosity level and the range of pore sizes observed from the CT scans. For now the pores are considered to have sizes between 100 - 300 μm, with further updates on the range to come when new scans are done. Based on these assumptions, for HA0B which has a porosity of 53.33%, E is 25.5% of the Young's Modulus of the solid material. This is the model used in finding E for all samples described in Section 2 and for the theoretical calculations and simulations below.

4 THEORY

The theoretical apparatus upon which the calculations in this section are based can be divided into three parts described below.

Firstly, sandwich beam bending theory gives sample deflection under a bending load and is covered in detail by Allen[11].

Secondly, honeycomb sandwich theory (both 3PB and compression) identifies the main failure modes and provides calculations for the sample failure load for each mode. Covered by A. Petras and M.P.F Sutcliffe[12] on the one hand and Zhang and Ashby[13] (mainly compression) on the other. Note that for local indentation in 3PB, Zingone's elastic beam in an elastoplastic medium model[14] was used.

Finally, honeycomb mechanics since in order to evaluate the honeycomb failure mechanisms, the honeycomb stiffness, strength and density are needed. They were determined as a function of the base solid material properties by Zhang and Ashby[13] and Wierzbicki[15].

Based on the theoretical relations found in the aforementioned papers, a set of theoretical predictions could be put together for four of the seven sample types listed in Section 2. The three samples that stray significantly from theory in terms of geometry are HA1B, HA2B and HA3B. However, HSNB/HSNC and HA0B/HA0C will be able to give the underlying behaviour of both a baseline sandwich panel and one with a printed core.

In 3PB, all failure modes can be evaluated and the one with the lowest failure load is predicted to dominate in a real life experiment. This gives the strength prediction, while the sample deflection under the experimental failure load will give the stiffness prediction.

The stiffness solution varies linearly with geometrical parameters that should be well-known (sample size/height) and with Young's Modulus (E) and Shear Modulus (G). For the baseline honeycomb, E and G are given by data sheets, while for the printed version, the high porosity level of the AlSi10Mg samples makes it more difficult to predict these properties, as was discussed in Section 3.

The strength solution is in a similar situation, since no failure mode is particularly sensitive to any material property or sample dimension. Some properties like τ_{31} and τ_{32} (core shear stress in directions 31 and 32) do vary with the cube of the honeycomb density ratio, so it seems like the solution may be sensitive to wall thickness. However, even if locally some walls may vary in thickness, globally the density should be close to spec (for standard Hexcel honeycombs the density tolerance is 10%[16] [17]). The relevant material properties are known for HSNB, while for HA0B they have to be inferred from theory, making the predictions less reliable. Overall, the bending predictions are expected to follow experimental values quite closely especially for HSNB. The results for HSNB and HA0B are in Table 6.

For both HSNB and HA0B, the failure mode predicted is local indentation. From the experimental data, HSNB does fail through local indentation at a load of 1252.2 N, just 5.8% higher that the predicted load. On the other hand, HA0B fails through top facesheet yielding, which is the second predicted mode in theory and it occurs at a load 31.9% higher than in the experiment. Given the uncertainties regarding the material properties of the printed material, the prediction is deemed reasonable.

In terms of sample stiffness, it was expected for theory to predict a higher stiffness compared to the experiments due to the imperfections of the real samples. Indeed, HSNB has a predicted deflection 47.53% lower than observed, while HA0B has a predicted deflection 25.3% lower than observed.

In compression, the theoretical prediction for both elastic and plastic buckling load varies with the cube of the honeycomb wall thickness. As opposed to bending, where local thickness variation is insignificant compared to the global density, compression depends on the local behaviour. This makes the solution very sensitive to a geometrical parameter that can greatly significantly in real life due to manufacturing tolerances. Moreover, the buckling load can vary significantly between two seemingly identical samples due to local imperfections, once again related to manufacturing. These factors make buckling load prediction a lot less reliable compared to 3PB strength and stiffness prediction.

Sample	Face Yield (N)	Intra-cell Buckling (N)	Face Wrinkling (N)	Core Shear (N)	Local Indentation (N)	Deflection (mm)
HSNB	5810.1	38297	21823	1953.9	**1183.6**	0.35952
HA0B	**5981.2**	39424	42079	74711	**1518.4**	0.74605

Table 6: Theoretical Predictions for 3PB samples. Relevant values in bold.

The results for HSNC and HA0C are as follows:

Sample	Plastic Buckling Load (N)	Elastic Buckling Load (N)
HSNC	2724.15	5298.46
HA0C	15707	231501

Table 7: Theoretical Predictions for compression

In general, it is expected for the predicted buckling load to be higher than the experimental one because of the important effect of manufacturing imperfections. However, for HSNC both the predicted plastic and the elastic buckling loads are lower than their experimental counterparts: by 22.2% compared to the plastic buckling load of $\approx$ 3500 N from Figure 3 and by 34.6% compared to the elastic buckling load of 8102 N reported before. This leads to the probable conclusion that the reported honeycomb wall thickness was lower than on the manufactured sample. Because the buckling load scales with the cube of the wall thickness, a 15% increase in wall thickness (from 18 μm to 20.7 μm) would match the predicted and experimental elastic buckling loads. The difference is probably a little higher since imperfections will bring the buckling load down, but the point remains that the variation between theory and experiment is well within experimental variations due to manufacturing errors.

For HA0C, theory grossly over-predicts the plastic and elastic buckling loads (by 314% and 1123% respectively). This was expected since the 3D printed samples have relatively thick walls (0.3 mm) which will bring the theoretical value up, while being filled with porosity and imperfections which will significantly lower the experimental value. The porosity is accounted for in the value of Young's Modulus, but the effect of porosity on the effective wall thickness is unknown.

Overall, honeycomb theory does a good job of giving insight into the behaviour of both baseline and printed sandwich constructions under bending and compression. The theory has qualitative value in the sense that it underlines the material properties and geometrical features that influence structural performance the most, while having quantitative value in predicting most of the strength/stiffness characteristics within reason.

5 SIMULATION RESULTS

The FEA investigation done on the experimental samples had a few main objectives: to understand the relative effect of geometrical parameters on sample performance; to get insight into the relative role of material properties on sample performance; to understand how friction changes the experimental/simulation results in 3PB; to discover how simulations compare to experimental and theoretical results and why. This will help predict future experimental performance of samples that are initially analyzed through FEA.

In a sandwich construction with a honeycomb core, the most difficult part to model correctly is the honeycomb because of its very thin walls. Thin-walled structures are generally best described by shells, either with 4 or 8 nodes, depending on application. Solids can be used as well, but in general it is advisable to have 6 to 10 solid elements through the wall thickness in order to correctly capture the linear variation of strain across the thickness. On the other hand, only one shell element is needed through the thickness and the element size can be easily 10 times larger than the wall thickness. As a result, shells will be significantly more computationally efficient. Furthermore, varying geometrical parameters easily is desirable in order to assess how the output varies since manufacturing dimensions are likely to differ from the design.

The CAD would be turned into a mesh of less accurate solid elements and it would be very time consuming to update because of the complex geometry. On the other hand, especially with ANSYS APDL, a model can be built from start to finish by writing a series of commands in a text file, which makes it easier to update and rerun a model. Moreover, since shells do not have a physical thickness, but a user defined one, one can vary the wall thickness of a certain honeycomb construction by just adjusting the shell settings, rather than by entirely redesigning it in CAD. As a result, building the geometry in the FE solver using shells for the honeycomb walls is preferred to building a CAD model and then importing it to the FE solver with a Solid based mesh.

The software of choice was ANSYS APDL because of previous knowledge with it and because the entire simulation from pre-processing to post-processing can easily be setup in a command text file. However, some preliminary work focused on fixing simulation parameters such friction coefficient was done in ANSYS WorkBench (WB). The CAD was readily available and the workflow was fast in establishing these parameters that were later used in the APDL simulations. Moreover, HA1B/HA2B/HA3B were solely investigated in WB because replicating their more complex geometry in APDL would be very time consuming. For these simulations, Solid 186 was used because it has quadratic displace-

ment which means it will exhibit linear strain even if only one element is used through the thickness. Details of the analysis can be found later on in this section.

5.1 Three Point Bending

The three point bending model is a quarter of the experimental setup since it makes use of symmetry along the cross-head (Y-Z plane) while in the X-Y plane, symmetry caused issues (see Figure 7). However, it was quickly verified that a full model and a model cut in half along the X-Y plane behave virtually the same due to the periodic nature of the structure. The model is made up of the CFRP facesheets, the Aluminium honeycomb (standard or printed), a cross-head applying the load and the support leaving a free half-span of 75 mm. The element types used for each component and the reasoning behind the choices are described below.

For honeycomb walls Shell 281 is used. Both Shell 181 (4 node element) and Shell 281 (8 node element) are appropriate since both can employ full integration for the in-plane bending that will occur in the honeycomb walls. For these models, the run-time difference between 181 and 281 is insignificant, so Shell 281 was used.

For CFRP facesheets Solid 186 is used. Initially, Shell 281 was picked because the facesheets are thin and shells are the most appropriate for modelling. However, issues came up when adding friction between the facesheets and the supports and they were resolved by using solid elements. The trade-off is advantageous because while the run-time and accuracy differences are insignificant, the addition of friction to the model is essential as will be discussed later.

For the cross-head and support Solid 186 is used. Both have relatively large dimensions in all directions, so a solid element is most appropriate. They make up a small fraction of the model, so they do not significantly increase the run-time.

The next issue to be established was the contact area between the support/cross-head and the CFRP facesheets. This is because both the cross-head and the support are cylindrical and theoretically they will have a point contact with a flat surface, but in reality a contact width can be observed. By investigating images from the experiments, a contact width of around 3.5 mm was established. The impact of the contact width on the sample deflection was investigated in Ansys WB. It was found that the vertical deflection varies by around 0.1% for a contact size between 0 and 3.5 mm. In the end, a contact width of 2.38 mm (half the honeycomb cell size) was used to accommodate both the real life observation and the node merging issues in APDL while not compromising on accuracy.

Moving on from contact width, significant sliding between the sample and the supports was observed in the experiments and an appropriate friction coefficient had to be established (see Figure 6). Once again, a preliminary study was done in Ansys WB to find the vertical displacement variation with the friction coefficient used. For $\mu_f \in [0.02,\ 0.15,\ 0.35]$ the variation was less than 5%, but by comparison, the bonded model deflects 30% less. There is a clear indication that having the sample bonded to the support is unrealistic and also that finding the exact friction coefficient is not essential.

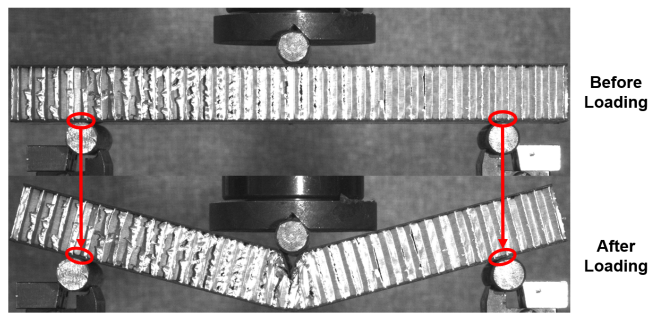

Figure 6: One of the HSNB samples under 3PB. Notice how the sample slides relative to the supports.

A good guess at this friction coefficient can be taken from known values of μ_f for stainless steel (support) sliding on CFRP (facesheet). The value is around 0.15[18] and even though it will vary based on surface finish, it is a good middle-of-the-road initial guess. An investigation into the friction coefficient impact on 3PB experimental results was done at the Politecnico di Milano[4] in 2012, but it focused solely on the friction between cross-head and sample and its impact on sample failure. The conclusion was *"that the local indentation under the puncher is strictly connected with friction"*[4] and that μ_f should lie between 0 and 0.3 for their steel puncher - Al2024-T3 skin setup. As a result, it was decided that a friction coefficient of 0.15 can be reliably used both between the bottom facesheet and the support and between the top facesheet and the cross-head.

Finally, material properties come into question. The CFRP and the standard baseline honeycomb have known properties provided in data sheets, while the 3D printed Aluminium core properties were determined as described in Section 3.

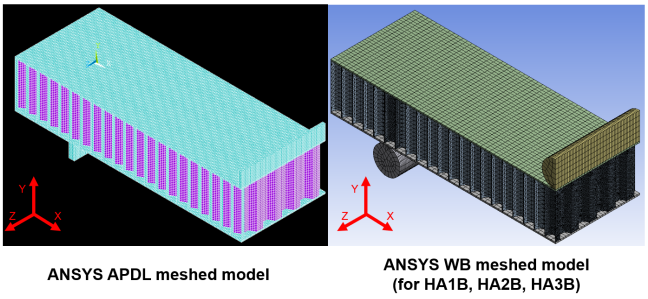

Figure 7: FEA models built in ANSYS APDL and ANSYS WB for 3PB simulations

For node merging purposes, the element sizes used for the facesheets and for the honeycomb faces depend on each other and on the honeycomb cell size. Let the honeycomb cell size be equal to L. If the honeycomb double walls have an element size of L, the askew walls should have an element size of $2L$ and the facesheets an element size of L in the direction parallel to the double walls by $L/\sqrt{3}$ in the direction normal to the double walls. With this in mind, the element sizes used are: $L/2\sqrt{3}$ by $L/4\sqrt{3}$ for the honeycomb faces and $L/4$ by $L/4\sqrt{3}$ for the facesheets. Here, L is 4.7625 mm. Vertical displacement varies by 2.1% between this model and one with double the element size, so the solution is considered to be converged. Moreover, the computational time increases significantly if one uses smaller sizes.

Before presenting the results, it must be explained why the HA1B/HA2B/HA3B analysis done with Solid 186 elements in ANSYS WB is relevant. A comparison was made between similar simulations done in APDL with the setup described above and in WB and differences of less than 10% were found in terms of vertical displacement results. It is desirable to build all models in the same way, but for these samples it was deemed faster to solve in WB with minimum accuracy detriments. Since in WB the part contacts are solved by default, there are no restrictions on the relative element sizes. As a result, an element size of 2 mm was used for the facesheets and support/crosshead, 1.5 mm for most of the honeycomb and 0.5 mm on the honeycomb under the crosshead and above the support.

Note that the load applied on the samples from Table 8 is the experimental average sample failure load reported in Table 2.

Based on Table 8, the baseline core and the standard printed structure are both around 60% stiffer in the simulations compared to the experiment. This was expected since the simulation employs perfect contacts whereas in reality the quality of the core - facesheet contact varies and is imperfect. The simulated models seem to have captured the underlying mechanics of the 3PB loading case as their experimental relative performance holds in the simulations. This means that the main differences between the two were captured through the wall thickness variation and through the material models used.

Sample	Vertical Displacement (mm)	Sample stiffness (N/mm)	Sample specific stiffness (N/(mm × g))
HSNB	0.423	2960.198	71.972
HA0B	0.64	7085.444	90.008
HA1B	0.624	7791.641	93.515
HA2B	0.621	8832.67	91.021
HA3B	0.746	10226.888	88.094

Table 8: 3PB simulation results for honeycomb samples under experimental failure load

The samples with increasing adhesive area are on average 28.53% stiffer in the simulations compared to the experiment. The results are closer between simulation and experiment than for the previous samples. In the case of the printed cores, this may be because the samples with more adhesive contact area have increasingly less porosity, which may bring the FEA model closer to reality. Moreover, the experimental samples approach a perfect contact as the contact area increases and will behave closer to the ideal conditions in the FEA model.

The experiments show that the regular printed core performs worse than all the samples with more adhesive contact area, while the simulations show it behaves very similarly. This means that the FEA model does not capture the effect of increased adhesive area. The core is perfectly bonded to the facesheets in the simulation, while the real samples might suffer from imperfect bonding which will be more acute for less contact area. As a result, regardless of contact area, all FEA models behave roughly the same in terms of sample specific stiffness, while the experiments show a distinct improvement up to 50% contact area.

5.2 Compression

The compression model was built in a similar way to the 3PB model, but friction is not a relevant factor anymore. The bottom facesheet was simply constrained in all degrees of freedom (DOF) and a block made of Solid 186 elements applied the load on the samples. This way the top facesheet is constrained and it transfers all loads to the core.

Once again, a quarter model was employed, but applying symmetry caused issues. In order to make sure that accuracy was upheld without symmetry, the buckling load was compared between two similar models with different honeycomb cell numbers. It was discovered that for the same element size, the buckling load only varies by 6.5% between a full and a quarter model, but the quarter model is 94% faster (6 minute solve time vs 101 minutes). As a result, it is sensible to use a quarter model with no symmetry. The full model represents the entire experimental compression sample.

The element sizes that can be used both on the core walls and the facesheets are related to one another in order for the top and bottom honeycomb nodes to be merged to the facesheet nodes. With these constraints in mind, a convergence study was done both on a single cell model and on the quarter model to see if convergence would vary with model size. An element size of $L/12$ by $L/12\sqrt{3}$ for the facesheets and $L/6\sqrt{3}$ for the core was deemed appropriate since the buckling load changes by less than 1.5% for both if the element sizes were decreased a further 33%. Once again, L is 4.7625 mm. The results for this setup are in Table 9.

Sample	Elastic Buckling Load (N)	Vertical Displacement at Experimental Buckling Load (mm)
HSNC	930.6	0.034
HA0C	74568.25	0.115

Table 9: Honeycomb compression simulation results

Similar to the discrepancy between experiment and theory, the simulations also underpredict the HSNC buckling load and grossly overpredict the HA0C buckling load. This is a sign that for the standard baseline core, the honeycomb walls are likely to be thicker compared to the data sheet, while for the printed core the weakening effect of the pores is not fully captured. The HSNC simulated buckling load is 11.49% of the experimental value, while the simulated value for HA0C is 3.6 times larger than in the experiment.

In terms of the sample deflection, HSNC deflects 37% less than in the experiments, while HA0C deflects 6.1 times more in the simulation compared to the experiment, for the same load. Given the uncertainty regarding experimental deflection data for compression, it is difficult to judge this comparison quantitatively. Qualitatively, the sample deflection provides an opposing trend compared to the buckling load. HSNC is weaker in the simulation, but stiffer, while HA0C is significantly stronger in the simulation, but a lot less stiff. This contrast suggests that the standard baseline core absorbs a lot more energy in real life than in the FEA model, while for the printed core the opposite is predicted. More needs to be understood regarding the printed core properties and the effect of imperfections on its performance to be able to model its energy absorption under quasi-static loads more accurately.

6 RESULTS CONCLUSION

A summary of the relation between experimental results and theoretical/simulation predictions is given in Table 10.

On average, for HSNB and HA0B, both theory and simulation predict a sample deflection around 37% less than the experimental value. The relation between experiment, theory and simulation is similar for both which gives confidence that sample performance on paper can be scaled reliably to predict experimental performance.

Sample	Theoretical Values	Simulation Values
HSNB	$\Delta y_{th} = 0.525 \times \Delta y_{exp}$	$\Delta y_{sim} = 0.618 \times \Delta y_{exp}$
HA0B	$\Delta y_{th} = 0.747 \times \Delta y_{exp}$	$\Delta y_{sim} = 0.641 \times \Delta y_{exp}$
HA1B	N/A	$\Delta y_{sim} = 0.763 \times \Delta y_{exp}$
HA2B	N/A	$\Delta y_{sim} = 0.855 \times \Delta y_{exp}$
HA3B	N/A	$\Delta y_{sim} = 0.727 \times \Delta y_{exp}$
HSNC	$F_{th} = 0.654 \times F_{exp}$	$F_{sim} = 0.1149 \times F_{exp}$
HA0C	$F_{th} = 11.231 \times F_{exp}$	$F_{sim} = 3.618 \times F_{exp}$

Table 10: Results comparison to experimental data

In the case of the honeycombs with varying adhesive contact area, while the simulation results are close to the experimental value, the FEA models do not convey the advantage of having an increased contact area. The contact imperfections of the real samples are likely to be more significant the smaller the contact area, thus leading to HA0B performing significantly worse than HA2B as opposed to the simulations where they are very similar. This is an indication that more work needs to be done to capture these performance differences. Even though a single sample of these three types was produced, they are all versions of the same experiment and they show consistent behaviour removing the concern for an outlying performance.

The compression samples have opposing trends, with HSNC being stiffer in reality while HA0C is considerably less stiff than predicted. For both, theory overpredicts the sample stiffness compared to the simulation, which is

expected since the theory assumes fully constrained ends for the honeycomb walls, while reality is somewhere in between a built-in strut and a pinned join. One needs to better understand the effect of porosity on the effective load bearing thickness of printed honeycomb walls.

Both theory and simulation do a good job of predicting sample performance in 3PB. However, in compression the wall thickness of the core dominates along with local defects. This makes experimental results more prone to being influenced by the many manufacturing defects of thin-walled cores. The effect of these faults needs to be included in the FEA and theoretical models.

To conclude, this investigation shows that 3D printed honeycomb cores have the potential to outperform standard baseline Aluminium cores in both 3PB and compression. With the added opportunity to vary the design along the printed core to optimize load spreading, 3D printed honeycomb cores can lead to significant performance improvement and mass saving. Some of the challenges involving porosity were also discussed and tackled and valuable experimental data was gathered to begin quantifying the effect of porosity on the mechanical properties. Manufacturing inconsistencies and sample defects need to be addressed in order to arrive at a set of consistent prints of high structural performance. More work needs to be done in this area along with accounting for more sample defects in FEA modeling.

Acknowledgements

The experimental work reported was funded through the European Commission Horizon 2020, Framework Programme for Research and Innovation (2014-2020), under the ReDSHIFT project (grant agreement n. 687500).

7 References

[1] Dunbar B. Advanced Space Transportation Program fact sheet. `https://go.nasa.gov/393UcPm`, Apr 2008, Accessed Jan 2021.

[2] Haydn N.G.W. *Multifunctional periodic cellular metals. Philosophical Transactions of the Royal Society A: Mathematical, Physical and Engineering Sciences*, 364(1838):31–68, 2006.

[3] Romei F., Rumpf C., and Walker S.J.I. *ReDSHIFT - 3D Printing Design Strategy.* Technical report, 2019.

[4] Giglio M., Giglioli A., and Manes A. *Numerical investigation of a three point bending test on sandwich panels with aluminum skins and Nomex™ honeycomb core. Computational Materials Science*, 56:69–78, 2012.

[5] Choren J.A., Heinrich S.M., and Silver-Thorn M.B. *Young's modulus and volume porosity relationships for additive manufacturing applications. Journal of materials science*, 48(15):5103–5112, 2013.

[6] Smith J., Xiong W., Yan W., Lin S., Cheng P., Kafka O.L., Wagner G.J., Cao J., and Liu W.K. *Linking process, structure, property, and performance for metal-based additive manufacturing: computational approaches with experimental support. Computational Mechanics*, 57(4):583–610, 2016.

[7] Eshelby J.D. *The determination of the elastic field of an ellipsoidal inclusion, and related problems. Proceedings of the royal society of London. Series A. Mathematical and physical sciences*, 241(1226):376–396, 1957.

[8] Luo J. and Stevens R. *Micromechanics of randomly oriented ellipsoidal inclusion composites. Part II: Elastic moduli. Journal of applied physics*, 79(12):9057–9063, 1996.

[9] Vavakin A.S. and Salganik R.L. *Effective characteristics of nonhomogeneous media with isolated inhomogeneities. Mechanics of solids*, 10:58–66, 1975.

[10] Manoylov A.V., Borodich F.M., and Evans H.P. *Modelling of elastic properties of sintered porous materials. Proceedings of the Royal Society A: Mathematical, Physical and Engineering Sciences*, 469(2154):20120689, 2013.

[11] Allen H.G. *Analysis and design of structural sandwich panels.* Elsevier, 1969.

[12] Petras A. and Sutcliffes M.P.F. *Failure mode maps for honeycomb sandwich panels. Composite structures*, 44(4):237–252, 1999.

[13] Zhang J. and Ashby M.F. *The out-of-plane properties of honeycombs. International journal of mechanical sciences*, 34(6):475–489, 1992.

[14] Zingone G. *Limit analysis of a beam in bending immersed in an elastoplastic medium. Meccanica*, 3(1):48–56, 1968.

[15] Wierzbicki T. *Crushing analysis of metal honeycombs. International Journal of Impact Engineering*, 1(2):157–174, 1983.

[16] Hexcel. *HexWeb CR3 Corrosion Resistant Specification Grade Aluminium Honeycomb*, 2017.

[17] Plascore. *PAMG-XR1 5056 Aluminium Honeycomb*, 2019.

[18] Friction and Friction Coefficients. `https://bit.ly/3j67iA2`, Accessed Jan 2021.